Scientific paper

Numerical Analysis of Flow and Segregation of Self-Consolidating Concrete During Casting of Reinforced Elements

Wei Chen[1], Zhuguo Li[2*] and Caijun Shi[3,4]

Received 20 June 2024, accepted 14 November 2024 doi:10.3151/jact.22.735

Abstract

It is well known that whether self-consolidating concrete (SCC) can be self-consolidated mainly depends on its flowability and segregation resistance. The shape and grading of coarse aggregate (CA) particles, as well as the arrangement of reinforcing bars, are two of the main factors influencing these properties. In this study, we developed a new meshless particle method that can reflect the influences of CA shape and rebar on concrete flow and segregation behavior during casting reinforced elements. Fresh concrete was represented by irregular CA particles and spherical mortar particles. CA particles were formed by small elementary particles (EP) to have their actual sizes and shape index. Then, the flow and segregation behaviors of two kinds of concrete in an L-shaped box with rebars were investigated experimentally and numerically, respectively. As a result, compared to the original double-phase & multi-particle (DPMP) method, the proposed numerical method improves the simulation accuracy by approximately 30% for flow behavior, and 20% for segregation behavior, respectively, during casting reinforced SCC using crushed stone as CA with poor shape, however, shows only a slight improvement when simulating the flow and segregation behaviors of SCC using artificial aggregate as CA with nearly spherical shape.

1. Introduction

With the development in chemical and mineral admixtures, new kinds of concrete such as self-consolidating concrete (SCC) (Ozawa 1989) and high-strength concrete have been developed and put into practice for easy construction and high structural quality. SCC can fill mold under gravity without vibration, speeding up the concrete casting process and saving energy. However, despite these obvious advantages, SCC has not been widely used. One of the serious challenges is how to design SCC to ensure that it has suitable fluidity and segregation resistance for achieving self-compaction, and how to judge whether it can be self-compacted or not.

During SCC placement, it passes through the dense reinforcement and finally fills everywhere in the formwork. Besides high fluidity, SCC should maintain an even distribution of coarse aggregate (CA) in matrix mortar (ACI 2007; Khayat and Mitchell 2009) after flowing. Good workability of SCC not only depends on the fluidity and segregation resistance of fresh concrete but also is related to reinforcement, shape, and size of the concrete member, construction method, etc. To evaluate the workability of high fluidity concrete, slump flow test, J-ring test, U-shaped box test, etc. have been used. However, the results of these tests are only associated with specific features of fresh concrete under specific conditions (Li *et al.* 2021), thus they cannot necessarily reflect the real flow behavior of concrete during the actual construction process. Large-scale field experiment is a solution for confirming the workability of fresh concrete, but it is time-consuming, laborious, and expensive (Xu *et al.* 2021; Wang *et al.* 2022). Therefore, the numerical flow simulation-based workability evaluation has been proposed for fresh concrete (Tanigawa and Mori 1988; Li 2007). This method is considered an integrated approach, as it comprehensively considers the properties of fresh concrete as well as the construction and structural conditions.

More than one-third of the volume of concrete is coarse aggregate (CA), of which characteristics such as shape, particle size distribution, and density have a profound influence on the properties of fresh concrete (Zhao *et al.* 2021). It is well known that the rounder the shape of aggregate particles, the higher the fluidity of fresh concrete, but the lower the resistance to segregation (Li 2014). Hu and Wang (2011) found that for a given matrix mortar, the yield stress and plastic viscosity of fresh concrete increase with the increase in the void ratio and the frictional angle of CA, but decrease with the increase in the size of CA. Zhao *et al.* (2021) reported that removing the particles with small flatness and large roughness from CA can largely increase the fluidity of fresh concrete. Cepuritis *et al.* (2016) also found that a higher flakiness index (poor shape) results in a lower slump. Therefore, to

[1]Ph.D candidate, Graduate School of Science and Technology for Innovation, Yamaguchi University, Ube, Yamaguchi, 755-8611, Japan.
[2]Professor, Graduate School of Science and Technology for Innovation, Yamaguchi University, Ube, Yamaguchi, 755-8611, Japan. *Corresponding author,
E-mail: li@yamaguchi-u.ac.jp
[3]Professor, College of Civil Engineering, Hunan University, Changsha 410082, China.
[4]Visiting Professor, Graduate School of Science and Technology for Innovation, Yamaguchi University, Ube, Yamaguchi, 755-8611, Japan.

accurately simulate the flow of concrete, the shape of the aggregate must be considered.

Moreover, during the reinforced concrete casting, the presence of rebars may cause concrete blockage or aggregate segregation in the narrow gaps of rebars. Roussel *et al.* (2009) found that when concrete flows through rebars, the probability of aggregate blockage increases with the volume fraction of aggregate in the concrete, and the ratio of aggregate particle size to the clearance of rebars. Angular aggregates will increase the risk of forming granular arches between aggregates and rebars (Cui *et al.* 2020). Therefore, the occurrence of concrete blockage within rebars is greatly affected by the shape and grading of coarse aggregate (Roussel and Gram 2014). By the flow tests of SCC in an L-Box with and without steel bars, Roussel and Gram (2014) found that the steel bars harmed the fluidity of fresh concrete even in the absence of granular blocking. This is basically because fresh concrete is a kind of viscous granular material, not a pure liquid, thus when it flows between rebars, rebars will restrain the dilatancy that occurs with shear deformation, causing a decrease in the fluidity (Li and Li 2011).

Many meshless particle methods, such as the discrete element method (DEM) (Chu *et al.* 1997; Cao *et al.* 2017), the smooth particle hydrodynamics (SPH) method (Lucy 1977; Monaghan 1994; Sakihara 2004), and the moving particle semi-implicit (MPS) method (Koshizuka and Oka 1996; Yamada *et al.* 2020), are well applied to large deformation problems with free surfaces, including the flow of fresh concrete. The flow simulations of fresh concrete, using the DEM method and considering the shape of aggregate particles, have been reported (Roussel and Gram 2014; Cao *et al.* 2023). However, the parameters describing the interaction of discrete particles cannot be directly measured, needing calibration (Roussel and Gram 2014). The properties of freshly mixed concrete change with their formulations, thus the precise setting of the parameters is difficult for DEM, and the accuracy of the simulation is still questionable.

The MPS method uses an implicit algorithm to solve the pressure term, addressing the problem that the traditional SPH methods are not suitable for incompressible flows. However, the viscosity term is still solved using an explicit algorithm. To raise the efficiency and the solution stability of the MPS, Sun *et al.* (2012) and Xu *et al.* (2021) have improved the MPS by solving the viscosity term with an implicit algorithm. Furthermore, the harmonic mean inter-particle viscosity recommended by Shakibaeinia and Jin (2012), and the arithmetic mean particle density suggested by Duan *et al.* (2017) were incorporated in the improved MPS method of Xu *et al.* (2021) to improve the accuracy and stability of numerical results. This new MPS method is noted as I-MPS here.

By the traditional MPS, the segregation behavior of coarse aggregate in fresh concrete was analyzed based on the rheological properties of matrix mortar, the pressure gradient of fresh concrete, and the material segregation coefficient (Uehara *et al.* 2015). However, the interaction of coarse aggregate particles was not considered. The segregation behavior of coarse aggregate is not only dependent on the viscosity of fresh concrete (or the plastic viscosity of matrix mortar), but also influenced by the density, size, and shape of the coarse aggregates. On the other hand, Based on the I-MPS, Xu and Li (2021) further proposed a double-phase & multi-particle (DPMP) method to describe the fresh concrete for treating the CA segregation problem. The DPMP method treats fresh concrete as a two-phase fluid consisting of matrix mortar and CA particles, and is therefore able to consider the effects of CA particles' interactions and geometries on their segregation.

In this study, for developing a rational simulation method for the placement of self-consolidating concrete in the reinforced elements, we first improved the DPMP method to properly describe the grading and shape of coarse aggregate, and to consider the effects of rebar on the flow and segregation of fresh concrete. Then, the flow and segregation of the two high-fluidity concrete in an L-box with rebars were investigated experimentally and numerically, which used crushed stone and lightweight coarse aggregate, respectively. Finally, by comparing the numerical results with the experimental results of L-flow, the reliability and accuracy of the numerical approach developed in this study were validated. Based on the simulation results, the advantages of the improved DPMP method, compared with the single-phase fluid MPS method and the DPMP method, were discussed for different types of concrete, as well as the differences in the segregation behavior of lightweight aggregate concrete and normal aggregate concrete were examined quantitatively.

2. New numerical approach for fresh concrete

2.1 Algorithm of the I-MPS method

General MPS solves a pressure Poisson equation at every time step to ensure the incompressibility of the particle. The explicit algorithm is used to calculate the viscosity effect between the fluid particles, and the implicit algorithm is used to calculate the particle pressure. Hence, general MPS is called a semi-implicit algorithm (Xu *et al.* 2021). In this study, a complete implicit improved MPS (I-MPS) method (Xu and Li 2021) was utilized in our numerical approach. The implicit algorithms were employed to calculate both the viscous and pressure terms, Therefore, a large time step can be used to significantly improve the calculation efficiency.

The MPS or I-MPS method generally describes materials or fluids with the same virtual particles having the same dimension, and shape. In previous studies, fresh concrete has been commonly treated as a single-phase fluid, and it is typically represented using a single type of concrete particle, called the SPMP method (single phase and mono particle). For comparison, the SPMP method was also used in the numerical simulations of this study

described later. However, for predicting the segregation behavior of fresh concrete, the DPMP (double phase and multiple particle) method was proposed in our earlier study (Xu and Li 2021). In this method, fresh concrete is regarded as a two-phase granular fluid composed of matrix mortar and coarse aggregate (CA). As shown in **Fig. 1**, CA particles are formed with spherical elementary particles (EP). The formed CA particle has a spherical envelope, but not a sphere. The matrix mortar phase is represented by spherical particles with the same radius as EP. The density of CA particles and mortar particles is governed by the density of actual materials, respectively (Xu and Li 2021; Xu *et al.* 2024).

2.2 Numerical formation method of CA particles considering CA shape (SI/DPMP)

In the DPMP method, the number and fineness modulus (FM) of the formed CA particles are consistent with the actual volume and FM of CA used in the concrete, but the shapes of the formed CA particle cannot be controlled because EPs are randomly arranged. In this study, we further improved the DPMP method for making the formed CA has the same shape index (SI) as reality. Here, this improved DPMP method is noted as the SI/DPMP method.

As shown in **Fig. 2(a)**, we roughly classified the CA particles into six representative shapes and then assembled the EPs to get numerical CA particles with the six kinds of shapes, as shown in **Fig. 2(b)**. The surface area, volume, mass, and length of the short axis of each numerical CA particle were calculated respectively. The following relationships were established to calculate the number of numerical CA particles for each type of shape, which makes the numerical CA particles have the same volume, FM, SI, and PSD (particle size distribution) as the CA particles actually used in the concrete.

a) Total volume of numerical CA = Actual volume of CA in concrete
b) Shape index of numerical CA = Measured shape index of CA
c) FM of numerical CA = Measured FM of CA
d) Fraction of small numerical CA = Measured wt.% of small CA (5 to 10 mm)
e) Fraction of middle numerical CA = Measured wt.% of middle CA (10 to 20 mm)
f) Fraction of large numerical CA = Measured wt.% of large CA (> 20 mm)

In order to avoid the dispersion of EPs forming numerical CA particles during the flow of concrete, the Passively Moving Solid (PMS) model (Xu and Li 2021) is applied to calculate the movement of CA particles.

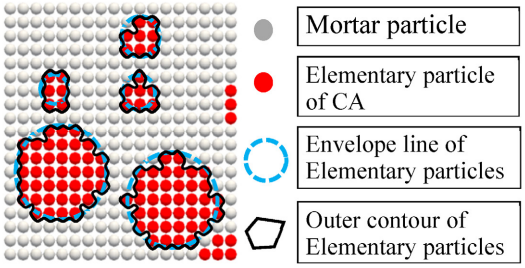

Fig. 1 DPMP method of concrete (2D).

2.3 Evaluation method of aggregate shape

Aggregate shape primarily involves three aspects: form (overall shape), roundness (large-scale smoothness), and surface texture, which are essentially independent of each other. Li (2014) proposed a simple shape evaluation method for aggregate, which integrates the above three aspects into a shape index by particle permeability test, according to Eqs. (1) and (2). These two equations show the evaluated result does not depend on the grading of particle assembly.

$$SI = \frac{6}{SS \cdot d_m} \tag{1}$$

where SI is the shape index, d_m is the average diameter of particles (m), and SS is the ratio of surface area to volume (m^2/m^3) of particles, which can be calculated by Eq. (2).

$$SS = \rho_S \cdot SS_m = \rho_S \cdot \sqrt{C \cdot \frac{g}{\eta_1 \cdot \rho_1 \cdot k \cdot D_r^2} \cdot \frac{e^3}{1+e}} \tag{2}$$

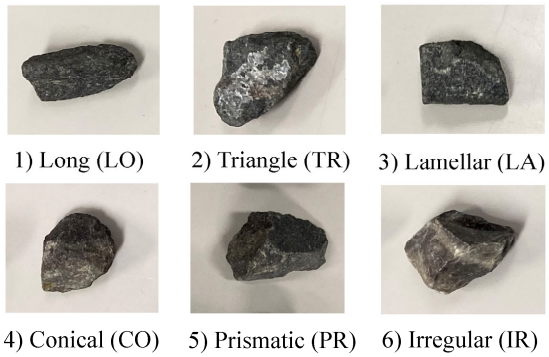

(a) Six representative shapes of crushed stone CA

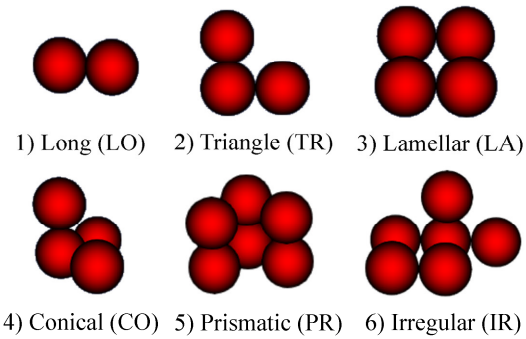

(b) Six kinds of assembled CA particle

Fig. 2 The SI/DPMP method for forming CA particle.

where ρ_s is dry density of aggregate (kg/m^3), η_l is viscosity of fluid used in the permeability test (N·s/m^2), ρ_l is density of used fluid (kg/m^3), SS_m is specific surface area (m^2/kg), D_r is ratio of density of particle to fluid, e is void ratio of particles, g is gravitational acceleration (m^2/s^2), C is a constant (0.5 for spherical particles), and k is the permeability coefficient measured by permeability test.

An example of a water permeability test device is shown in **Fig. 3**. However, in the case of the permeability test of coarse aggregate, if water is used, the flow of water is too fast to accurately determine the outflow rate. In this study, we used high-viscosity water glass with a viscosity of 142 (mPa·s) at 20°C instead of water to measure the permeability coefficient of the coarse aggregate. The detailed method for calculating the permeability coefficient k can be found in the work of Li (2014).

In Eq. (1), d_m can be determined by the fineness modulus of aggregate, but in this study, it was determined by the method described by Teranishi and Tanigawa (2007), as shown in Eq. (3).

$$d_m = \frac{1}{\sum_{n=1} \frac{(\ln D_{n+1} - \ln D_n)}{D_{n+1} - D_n} V_n} \tag{3}$$

where n is the number of sieves from the smallest opening size, D_n is nominal dimension of n^{th} sieve (mm), and V_n is volume ratio of aggregates in the n^{th} sieve.

2.4 Rheological model of fresh concrete

The Bingham model has been generally used as the rheological model of fresh concrete so far, which is simple with only two constants and describes the shear stress-shear rate relationship as a straight line. Nevertheless, ordinary concrete should be regarded as a viscous granular material with both fluid and granular characteristics. It is not doubtful that there are inter-particle friction, particle contact angle, and particle interlocking in fresh concrete. Therefore, the flow of fresh concrete is normally stress-dependent (Cao *et al.* 2019). However, the Bingham model cannot consider this normal stress-dependence. Recently, Li (2022) proposed the VGM model for granular fluid materials, which can describe the complex rheological behaviors of fresh concrete exhibited in the rheological experiments, including viscoelastic deformation before yielding, non-linearity of viscoplastic flow, shear thinning, and the dependence on normal stress and shear history. Compared to the Bingham model, the VGM model can contribute to a more precise numerical flow simulation of freshly mixed cementitious materials (Cao and Li 2017; Xu *et al.* 2021).

2.4.1 Simplification of the VGM model

The VGM model is shown in **Fig. 4**. In the viscoelastic deformation state (Stages I and II), there is a nonlinear relationship between shear rate and shear stress, as that in the viscoplastic flow state (Stage III). However, the viscoelastic deformation has little effect on the flow shape and distance of fresh concrete. Fresh concrete with high

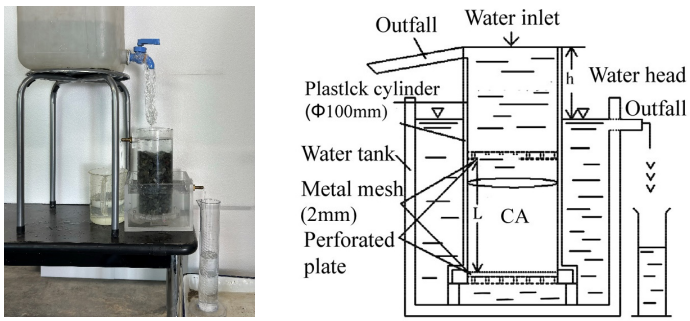

Fig. 3 Permeability test with constant hydraulic head.

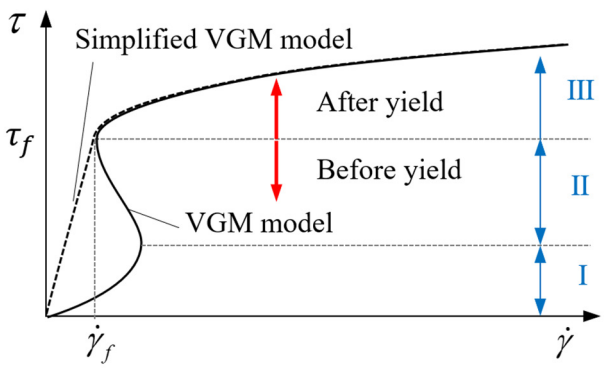

Fig. 4 VGM model and simplification.

fluidity may be subjected to a large shear stress exceeding its yield stress under its weight and thus enter the viscoplastic flow state directly in the beginning. Therefore, a precise calculation of viscoelastic deformation before yielding is not usually necessary in the numerical flow analysis of fresh concrete, particularly for high-fluidity concrete. We simplified the flow curve before yielding a straight line, as shown in **Fig. 4**, to raise computational efficiency and to solve the non-convergence problem, as a usual method (Zhu *et al.* 2010). Therefore, in this study, the simplified VGM model was used, as shown in Eqs. (4) to (7).

$$\begin{cases} \tau = \dfrac{\tau_f}{\dot{\gamma}_f}\dot{\gamma} \quad , & \tau < \tau_f \\ \tau = \tau_{yc} + \eta_c \dot{\gamma} \quad , & \tau \geq \tau_f \end{cases} \tag{4}$$

$$\tau_f = \sigma_n \tan(\theta_f + \phi_c) + C_{w1} \tag{5}$$

$$\tau_{yc} = \sigma_n \tan(\theta_f e^{-\kappa \cdot \gamma_i} + \phi_c) + C_{w1} \tag{6}$$

$$\eta_c = \frac{\eta_{0c}}{\cos(\theta_f e^{-\kappa \cdot \gamma_i})} \tag{7}$$

where σ_n is normal stress, θ_f is the mean particle contact angle at the yield point, K is a parameter related to shearing time-dependence, ϕ_c is the mean inter-frictional angle of fresh concrete, C_{w1} is shear resistance caused by mixing water's surface tension, τ_f is shear failure limit stress, $\dot{\gamma}_f$ is shear strain rate at the yield point, τ_{yc}, η_c are called apparent yield stress, and apparent plastic viscosity of fresh concrete, respectively, which change with shear strain, γ_i represents shear strain at time *t* in a viscoplastic flow state, and η_{0c} is a constant for a given concrete, called basic viscosity, only depending on environmental temperature, more details can be found in Li (2022).

2.4.2 Rheological constants for describing the interaction of matrix mortar particles

During the flow simulation using the SI/DPMP or DPMP method, the fresh concrete is regarded as a two-phase granular fluid. Therefore, the interaction of matrix mortar and CA particles should be considered separately.

Since matrix mortar has higher fluidity and is more homogenous, its granular characteristics are not obvious, compared with fresh concrete. If approximating the average particle contact angle (PCA) of mortar as zero, i.e., $\theta_f = 0$. τ_{yc} and η_c become two constants for a given concrete and a certain normal stress σ_n and temperature. Also, the shear resistance C_{w1} caused by the surface tension of mixing water was ignored in this study, because the water is almost saturated in mortar, thus the surface tension is very small. By simplifying Eqs. (6) and (7), the rheological model of matrix mortar in fresh concrete in the viscoplastic flow state was obtained, as shown in Eqs. (8) and (9).

$$\tau_m = \tau_{ym} + \eta_m \dot{\gamma} \tag{8}$$

$$\tau_{ym} = \sigma_n \tan \phi_m \tag{9}$$

where ϕ_m is the inter-frictional angle of mortar, τ_m is shear stress exposed to matrix mortar, τ_{ym} is the yield stress of matrix mortar, and η_m is the plastic viscosity of matrix mortar (equal to its basic viscosity η_{0m}).

2.4.3 Rheological constants for describing the interaction of CA particles

Since the CA particles are generated according to the actual shape, the effect of the CA particle's contact angle (PCA) does not need to be considered again in the rheological model. Thus, the mean PCA of CA particles was ignored in this study. Moreover, since a part of matrix mortar is tightly adhered to the surface of CA particles (Kennedy 1940; Xu and Li 2021), CA particle assembly containing mortar can be considered a special granular fluid. Therefore, by simplifying Eqs. (6) and (7), the rheological model of CA particle assembly can be expressed by a linear function, which has the same form as the Bingham model, as shown in Eqs. (10) and (11).

$$\tau_{CA} = \tau_{yCA} + \eta_{CA} \dot{\gamma} \tag{10}$$

$$\tau_{yCA} = \sigma_n \tan \phi_{CA} \tag{11}$$

where ϕ_{CA} is the mean inter-frictional angle of CA particle assembly, τ_{CA} is shear stress applied to CA, and τ_{yCA}, η_{CA} are yield stress and plastic viscosity of CA particle assembly.

However, there is currently no method to measure the above rheological constants of CA particle assembly. Many studies (Roscoe 1952; Krieger and Dougherty 1959; Struble and Sun 1992; Ferraris and De Larrard 1998; Ferraris *et al.* 2001) have found that the Bingham constants (plastic viscosity, yield stress) of fresh concrete are a function of the volume fraction of the solid phase and the maximum packing volume fraction of the solid phase. Therefore, the prediction equations of plastic viscosity and yield stress were suggested by Struble and Sun (1992), and Chateau *et al.* (2008), respectively, as shown in the following.

$$\eta_b = \eta_{bm} \cdot \left(1 - \frac{\varphi}{\varphi_m}\right)^{-\mu_* \cdot \varphi_m} \tag{12}$$

$$\tau_{by} = \tau_{bym} \cdot \sqrt{(1-\varphi) \cdot \left(1 - \frac{\varphi}{\varphi_m}\right)^{-\tau_* \varphi_m}} \tag{13}$$

where η_b and τ_{by} are estimated plastic viscosity and Bingham yield stress of fresh concrete, η_{bm} and τ_{bym} are measured plastic viscosity and Bingham yield stress of matrix mortar, φ is the volume fraction of CA in concrete, φ_m is the maximum packing volume fraction of CA, and μ_* and τ_* are intrinsic

viscosity and intrinsic yield stress of CA particle assembly, respectively.

For spherical particle assembly, the values of both μ_* and τ_* are 2.5. However, generally used coarse aggregate has an irregular shape. Therefore, the μ_* and τ_* of CA assembly should be calculated by Eqs. (12) and (13), based on the Bingham constants of matrix mortar and fresh concrete. Then, regarding the CA particle assembly with adhered matrix mortar as a special concrete (Xu and Li 2021), the rheological constants of CA particle assembly can be estimated by Eqs. (14) and (15). It should be noted that when considering the internal friction of fresh concrete or mortar, the measured Bingham yield stress of fresh concrete or mortar, corresponds to the normal stress caused by the mass of concrete or mortar sample used in the rheological test. Therefore, the measured yield stress (τ_{ym0}) of matrix mortar depends on the normal stress (σ_{nm0}) applied to the mortar during the rheological measurement.

$$\tau_{yCA0} = \tau_{ym0} \cdot \sqrt{(1-\varphi_{CA}) \cdot \left(1-\frac{\varphi_{CA}}{\varphi_m}\right)^{-\tau_* \varphi_m}} \tag{14}$$

$$\eta_{CA} = \eta_m \cdot \left(1-\frac{\varphi_{CA}}{\varphi_m}\right)^{-\mu_* \cdot \varphi_m} \tag{15}$$

where τ_{yCA0} is the estimated yield stress of CA assembly under the normal stress σ_{nm0}, η_{CA} is the estimated viscosity of CA assembly, τ_{ym0} is measured Bingham yield stress of matrix mortar, φ_{CA} is the volume fraction of CA particle assembly, containing the adhered matrix mortar, details about the φ_{CA} calculation can be found in Xu and Li (2021).

As shown in Eqs. (5), (9), and (11), the yield stresses of fresh concrete, matrix mortar, and CA particle assembly change with the normal stress. In the flow simulation, it can be considered that matrix mortar and CA particle assembly are subjected to the same normal stress (σ_n) with fresh concrete. Therefore, under the normal stress σ_n applied to the fresh concrete, the yield stress τ_{yCA} of CA particle assembly should be adjusted by Eq. (16), considering the density difference between CA and matrix mortar.

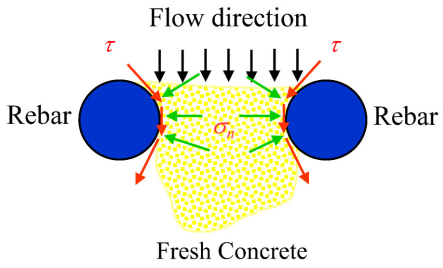

Fig. 5 Occurrence of normal stress in restricted shear flow.

$$\tau_{yCA} = \frac{\sigma_n}{\sigma_{nm0}} \frac{\rho_{CA}}{\rho_m} \tau_{yCA0} \tag{16}$$

where σ_n is normal stress applied to numerically analyzed fresh concrete, σ_{nm0} is normal stress applied to mortar samples during the rheological test of mortar, and ρ_{CA}, ρ_m are the densities of CA and mortar, respectively.

2.5 Restraint model of rebar and slippage boundary model

As explained earlier, reinforcement not only decreases the flowability of fresh concrete, but also may cause CA segregation, even concrete blockage. By the shear box experiments, Li and Li (2011) found that the shear resistance of fresh concrete increased when the horizontal shear deformation was freely induced, but the deformation in the vertical direction was restricted. They also detected a stress in the direction perpendicular to the shear direction. Thus, as shown in **Fig. 5**, we considered that when fresh concrete flows through the gap of rebars, the dilatant deformation is restricted by the rebars, thus an additional normal stress is led besides the one caused by the gravity of concrete. Eq. (17) expressed the relationship between normal stress and shear strain (Cao *et al.* 2019). In this study, the rebars are not only considered as static obstacles but also give a constraint to the fresh concrete. The constraint is expressed by a resulting normal stress, depending on the magnitude of shear strain and the feature of fresh concrete such as flowability, and grading and shape of aggregates.

$$\sigma_n = \begin{cases} \sigma_{n0} - a\gamma^2 + b\gamma, & \gamma < \gamma_f \\ \sigma_{n0} - a\gamma_f^2 + b\gamma_f, & \gamma \geq \gamma_f \end{cases} \tag{17}$$

where σ_{n0} is the initial normal stress of concrete before it enters the interval of rebars caused by the gravity of concrete, a and b are constants that relate to the rheological property and the granular feature of fresh concrete, γ is shear strain, and γ_f is shear strain limit at the yield point.

It is important to note that the magnitude of the additional normal stress generated between the rebars has a random nature and is influenced by the size and shape of coarse aggregate particles. The values of a and b in Eq. (17) obtained experimentally actually correspond to the averaged aggregate characteristics. Therefore, the present simulation approach using Eq. (17) only predicts the averaged flow and segregation behaviors of the whole concrete.

During the simulation, the concrete was restricted to flow in the L-box. In the MPS method, the L-box boundary is represented by three layers of boundary particles to ensure the particle number density during pressure calculation. The Dirichlet boundary condition (Galbusera and Niemeyer 2018) was adopted to solve the pressure Poisson equation. The pressure on the free surface was set to zero. The fresh concrete also suffers from boundary slip

Table 1 Properties of coarse and fine aggregates.

Physical property	Crushed stone	LCA	Sea sand
Surface dry density (g/cm^3)	2.72	1.68	2.57
Dry density (g/cm^3)	2.70	1.32	2.52
Water absorption (%)	0.84	27.0	1.82
Fineness modulus (FM)	6.68	6.44	2.52
Solid volume rate (%)	61.5	70.7	65.7
Shape index (SI)	0.52	0.88	-

resistance, we have adopted the visco-plastic model proposed by Murata and Suzuki (1987) to describe the slippage resistance, as shown in Eq. (18).

$$\tau_s = \eta_s v + \tau_{sy} \tag{18}$$

where τ_s is slippage-resistant stress at the boundary, η_s is the viscosity constant of slippage resistance, v is slippage velocity of particles, and τ_{sy} is yield stress of slippage.

3. Experimental program and numerical analysis

3.1 Raw materials used and mix proportions

As shown in **Fig. 6**, two kinds of coarse aggregate (crushed stone, and lightweight coarse aggregate (LCA): expanded clay) were used in the two high-fluidity concretes. Sea sand was utilized as fine aggregate. The properties of both the fine and coarse aggregates are shown in **Table 1**. The shape indexes of two coarse aggregates were measured by the permeability test using a water glass solution. The particle size distribution curves of aggregates are shown in **Fig. 7**. Ordinary Portland cement (OPC) with a specific surface area of 3500 cm^2/g and density of 3160 kg/m^3 was used as binder. JIS type II fly ash (FA) with a specific surface area of 4392 cm^2/g and density of 2300 kg/m^3 was used to replace 20% of OPC to add the viscosity of two concretes. A polycarboxylic acid-based AE super-plasticizer (SP) and a retarder mainly composed of sodium gluconate were also used for reducing the water content to improve the viscosity of fresh concretes and reducing the fluidity loss during the L-box flow test and the rheological tests, respectively. The mix proportions of two concretes are presented in **Table 2**.

(a) Crushed stone (b) Lightweight coarse aggregate

Fig. 6 Coarse aggregates used in two concretes.

3.2 Rheological properties of fresh concretes

Figure 8 shows the final shape of two concretes after the slump flow, and the results of the slump flow tests are shown in **Table 2**. The segregation was observed for both concretes, but the segregation patterns were different. In series No. 1 using the crushed stone, some CA particles are left in the center of the concrete sample to generate a central bulge. In series No. 2 using the LCA, the concrete was spread evenly but some of the LCA particles stopped on the concrete surface.

The VGM parameters and Bingham constants of the matrix mortar and the fresh concrete were measured by the RSNS rheometer, respectively. The detailed measurement method and the calculation methods for each parameter can be found in the work of Li (2015) and that of Li and Iidaka (2020). As described in Section 2.4.3, the

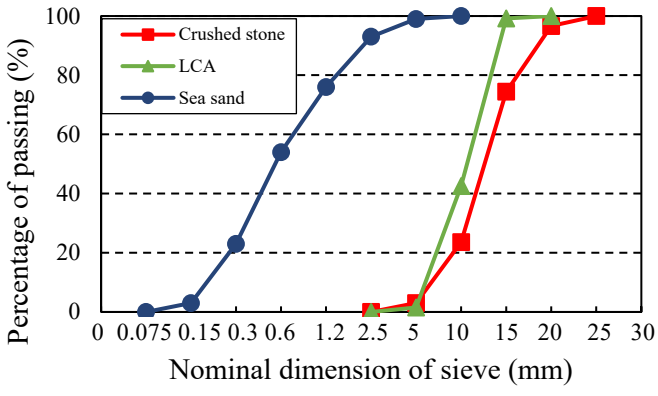

Fig. 7 Particle size distribution of aggregates.

Table 2 Mix proportions and properties of fresh concrete.

Series	w/b	Unit mass (kg/m^3)							V_{CA}	D_c	D_m	SL	SF	t_{500}
		Water	OPC	FA	Sand	CA	SP	Retarder						
No. 1	0.4	170	340	85	779	930 (CS)	4.9	4.25	34.2	2300	2150	24.5	576.5	2.6
No. 2	0.4	170	340	85	779	574 (LCA)	4.9	4.25	34.2	1876	2150	25.5	561.0	5.0

[Notes] CA represents coarse aggregate, CS is crushed stone, LCA is lightweight coarse aggregate, w/b is water-binder ratio by mass, SP is superplasticizer, V_{CA} is volume fraction of CA (%), D_c is bulk density of fresh concrete (kg/m^3), D_m is bulk density of matrix mortar (kg/m^3), SL is slump (cm), SF is slump flow (mm), and t_{500} is flow time of 500 mm (s).

Table 3 Rheological parameters of CA particle assembly.

CA assembly	Rheological parameters					Rebar restraint model constants	
	μ_*	η_{CA}	τ_*	τ_{CA0}	$\tan\phi_{CA}$	a	b
CS assembly	2.80	1679	7.43	772	2.4	1800	2000
LCA assembly	1.95	1336	3.47	524	0.8	2000	2200

Table 4 Rheological parameters of concretes and matrix mortar.

	VGM parameters							Boundary slippage model constants		Rebar restraint model constants	
	γ_f	η_0 (Pa·s)	$\dot{\gamma}_f$ (s^{-1})	K	θ_f (rad)	ϕ (rad)	C_{w1} (Pa)	η_s (Pa·s)	τ_{sy} (Pa)	a	b
No. 1	0.76	700	0.11	2.54	0.61	0.15	124.6	4.36	148	1090	1180
No. 2	0.38	430	0.07	1.38	0.20	0.10	88.9	4.36	145	1100	1200
Matrix mortar	0.23	172	0.13	1.87	0.09	0.12	76.1	2.41	102	-	-

intrinsic viscosity μ_* and intrinsic yield stress τ_* of two kinds of concrete were deduced, respectively, the VGM parameters of two kinds of CA particle assembly were calculated and shown in **Table 3**. The constants (a, b) of the boundary restraint model were proposed by matching the experimental and numerical results of the outflow rate of the V-funnel test (Cao *et al.* 2019). In this study, the a, b values were estimated for the concrete and the CA particle assembly based on the fluidity (slump flow, SF) of concrete, and the Bingham constants of the CA particle assembly, referring to the a, b values provided by Cao *et al.* (2019). The two constants in the boundary slippage resistance equation [Eq. (18)] were determined according to the method proposed by Murata and Suzuki (1987). All the rheological parameters were obtained for CA, matrix mortar, and concrete, as shown in **Tables 3** and **4**.

3.3 L-flow test and segregation measurement

An L-shaped box with rebars was fabricated with transparent vinyl chloride resin and round rebars for the L-flow experiment of fresh concrete. As shown in **Fig. 9**, the section and height of the vertical room are 200 × 200 mm, and 600 mm, respectively, and the length of the horizontal room was 800 mm. 3 columns and 3 rows of rebars with 10 mm diameter were installed in the horizontal room, the spacing between two rows of rebar is 200 mm, and the same row of rebar is spaced 42.5 mm apart.

After 24 liters of fresh concrete was filled into the vertical room of the L-box and kept standstill for about 1 minute, the sliding gate lifted quickly within 2 to 3 s, and the fresh concrete flowed into the horizontal room under gravity. After the flow stopped, the shape of the top surface of the concrete in the L-box was photographed. Then, as shown in **Fig. 9**, the concrete was divided into four zones in the horizontal direction and marked as A, B, C, and D.

(a) Crushed stone concrete (No. 1) (b) LCA concrete (No. 2)

Fig. 8 Final shapes of two concrete after the slump flow test.

Table 5 Configuration information of particles.

Method		SPMP	SI/DPMP			DPMP		
		Concrete particle	CA particle	EP of CA	Mortar particle	CA particle	EP of CA	Mortar particle
No. 1	Number	24000	2142	8188	15812	3221	8011	15989
	Density	2.3	2.72	2.72	2.15	2.72	2.72	2.15
No. 2	Number	24000	2175	8193	15807	3221	8029	15971
	Density	1.88	1.68	1.68	2.15	1.68	1.68	2.15

Table 6 Numbers of CA particles with six types of shape.

	LO	TR	LA	CO	PR	IR
CS assembly	410	602	308	288	438	96
LCA assembly	903	-	615	-	657	-

The coarse aggregate in each part was sieved out to get the volume fraction in each part of concrete. We conducted the L-flow test for the concrete using the crushed stone three times to verify the accuracy of the numerical method.

3.4 Configuration of numerical simulation

The L-flow numerical simulation of each fresh concrete was carried out by the SI/DPMP method, DPMP method, and SPMP method respectively. Based on the comparative study by Xu and Li (2021), the Taylor-Couette flow simulations were done by using elementary particle diameters of 10 mm and 5 mm, respectively to determine the suitable size of fluid particles used in the simulation. Both simulated results demonstrated high consistency with the theoretical results. To achieve a balance between computational accuracy and efficiency, the diameter of EP was set to 10 mm in this study. For the SPMP method, 24000 particles were used to represent fresh concrete. For the SI/DPMP and DPMP method the volume fraction of numerical CA was 34%, the same as that of actual CA used in each concrete.

The numbers of CA and mortar particles used in the SI/DPMP and DPMP method are shown in **Table 5**. **Table 6** shows the number of CA particles for the six types of shapes used in the SI/DPMP method. The number of boundary particles is 32208, which were used to describe the L-shaped box, sliding gate, and rebars.

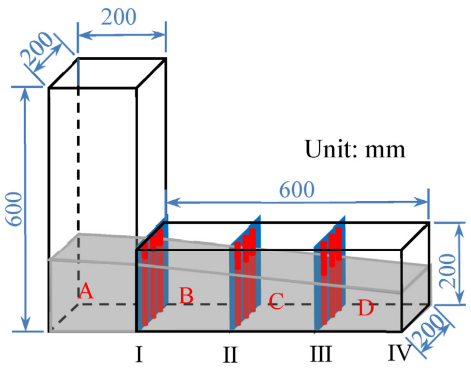

Fig. 9 Dimensions of L- box and concrete zoning.

4. Results and discussion

4.1 Flow behavior of fresh concrete in the L-shaped box with rebars

Figure 10 shows the height of concrete No. 1 at each position (marked as I, II, II, and IV, as shown in **Fig. 9**) for three repeated experiments, the mean value, and the standard deviation. It can be found that the three results at each position were very close, the maximum standard deviation was only 4.6 mm. Therefore, the L-flow test had a higher precision, even one experiment can measure precisely the flow shape of fresh concrete.

Figure 11 shows the differences in concrete heights at the four locations for the two concretes obtained by the SI/DPMP, DPMP, and SPMP methods, respectively. To quantitatively compare the simulation precision of the

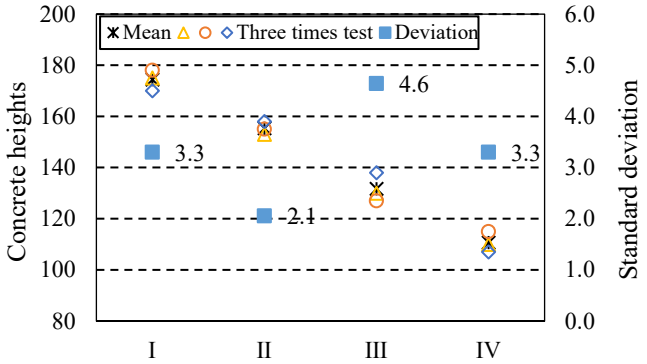

Fig. 10 Flow experimental results and standard deviation of No. 1 concrete.

Table 7 Deviation of simulation result compared to the experimental result.

	SI/DPMP	DPMP	SPMP
No. 1	4.6	6.6	6.9
No. 2	5.3	5.4	13.7

three simulation results, we calculated the deviation between the numerical results of each numerical method and the mean value of three times experimental results by Eq. (19) for each concrete. The calculated results are shown in **Table 7**.

$$R_e = \sqrt{\frac{\sum_{I}^{IV}\left(H_s^i - H_t^i\right)^2}{4}} \tag{19}$$

where H_s^i is concrete height obtained by simulation at location i, H_t^i is the mean height of concrete measured at location i with the locations being changed from I to IV.

From **Table 7**, it was found that for the LCA concrete (No. 2), the simulation results of the SI/DPMP and DPMP methods are closer to the experiment result than the SPMP method. Because in the SPMP method, fresh concrete was expressed by one kind of particle with the same density, the effect of the dynamic segregation of coarse aggregate in the horizontal direction could not be considered. As a result, the predicted precision of flow was reduced. The error values of the SI/DPMP method and DPMP method are almost the same, which are 5.3 and 5.4. This is mainly because the LCA particles are almost spherical or oval, as shown in **Fig. 6(b)**, thus they have a large shape index (0.88) close to the maximum value (1.0). The randomly formed CA particles by the DPMP method are near round or oval, as shown in **Fig. 1**. Thus, in the case of the LCA concrete, the DPMP method can provide the near simulation to the SI/DPMP method that intentionally forms CA particles according to the measured shape index of CA. As shown in **Table 6**, in the simulation of LCA concrete, only three well-shaped CA particles: LO, LA, and PR, were used.

However, for the crushed stone concrete (No. 1), the numerical analysis using the SI/DPMP method had the minimum error, compared with the other two methods, the SI/DPMP method improved the flow simulation accuracy by approximately 30%. It can be concluded that taking the shape of coarse aggregate into consideration can improve the accuracy of the flow simulation, especially for normal aggregate concrete. When the coarse aggregate particles have a good shape, similar to spheres, the effect of considering the shape in the flow simulation will be limited.

4.2 Flow pattern of concrete in the L-shaped box with rebars

To investigate thoroughly the flow behavior of crushed stone concrete in the L-box, the fresh concrete filled in the vertical room of the L-box was evenly divided into upper and lower layers. During the L-flow experiment, the mortar and aggregates in the upper layer were painted red, but in the lower layer were not colored. The obtained experimental result about the position change of two concrete layers at different time points are shown in **Fig. 12**. The red curves were drawn on the photos to represent the border between the upper and lower layers because mortar adhering to the front and back walls of the box reduced walls' visibility. The flow shape of the concrete at different times, velocity vector distribution at different positions, and the distribution of the upper and lower layers of concrete were also calculated by using the SI/DPMP method, as shown in **Fig. 12**.

As shown in **Fig. 12(a)**, after the gate of the L-box was lifted, the lower layer of concrete flowed rapidly into the horizontal room with a horizontal velocity. Large velocities of concrete particles can be observed at the upper surface and the front of the flow. As the concrete reached the

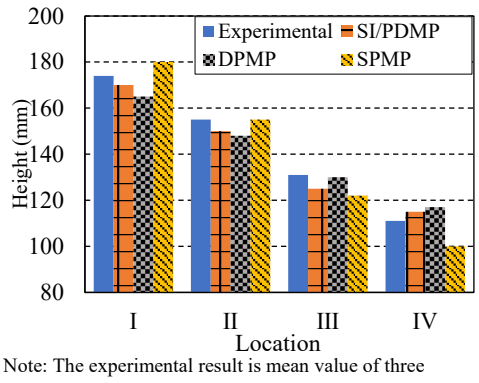

Note: The experimental result is mean value of three

(a) Crushed stone concrete (No. 1)

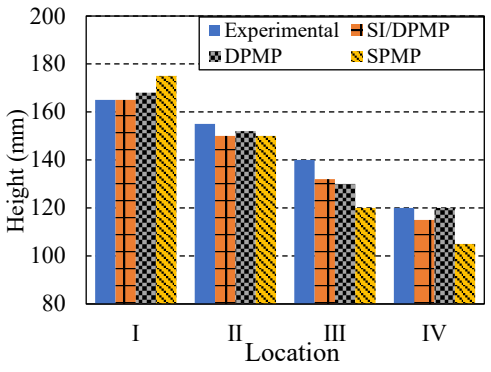

(b) Lightweight aggregate concrete (No. 2)

Fig. 11 Concrete heights at four locations.

Table 8 CA volume fraction (%) of concrete No. 1 in each zone and layer.

Zone		A			B			C			D		
Layer		Upper	Lower	Total	Upper	Lower	Total	Upper	Lower	Total	Upper	Lower	Total
Test times	1	30.4	34.1	32.2	31.4	38.2	34.7	30.1	35.3	32.5	30.4	30.9	30.7
	2	34.4	36.5	35.4	32.2	39.8	35.8	32.2	38.3	35.3	32.0	34.0	33.0
	3	32.2	35.4	34.0	33.1	39.0	36.1	32.4	36.4	34.4	31.4	34.9	33.4
Mean		32.3	35.3	33.9	32.2	39.0	35.5	31.6	36.7	34.1	31.3	33.3	32.3
Deviation		1.6	1.0	1.3	0.7	0.7	0.6	1.0	1.3	1.2	0.6	1.7	1.2

end of the horizontal room, the velocity direction of the front particles changed from horizontal to vertical and flowed upward under the inertia and the pressure of the rear concrete, as shown in **Fig. 12(b)**. Gradually, the rear concrete near the box bottom was pressed to flow to the front under the gravity of the above concrete and eventually stopped. Simultaneously, the upper layer concrete (red color) flowed slowly forward and consistently remained above the lower layer concrete (grey color). It is worth noting that the particles located in the lower left corner of the L-box moved have such a small velocity that there is no vector arrow in the lower left corner of the velocity vector distribution plots.

4.3 Segregation behaviors in the vertical and horizontal directions

To explore the CA segregation of concrete in the L-box with steel bars vertically, and horizontally, respectively, after the concrete flow stopped, as shown in **Fig. 10** the concrete was divided into four zones in the horizontal direction, and in each zone, the concrete was divided equally into the upper and lower layers. The volume of concrete in each part was measured, and then the CA was sieved out with a 5 mm opening sieve and washed off the adhering mortar. The volume of CA in each part in the surface dry state was measured. The volume fraction in each part was calculated based on the masses and densities of CA and concrete. **Table 8** presents the experimental results of concrete No. 1 at each zone and each layer. The average value and the deviation of CA volume fraction among the three experimental results were also given in **Table 8**, called the standard deviation for estimating the experiment error.

4.3.1 CA distribution in the vertical direction after the L-flow

As shown in **Figs. 13** and **14**, the CA volume fractions in the upper and lower layers of the two concretes in the four zones were measured, after the L-flow experiment or calculated from the L-flow simulation results.

According to the mix proportions of concretes, the CA

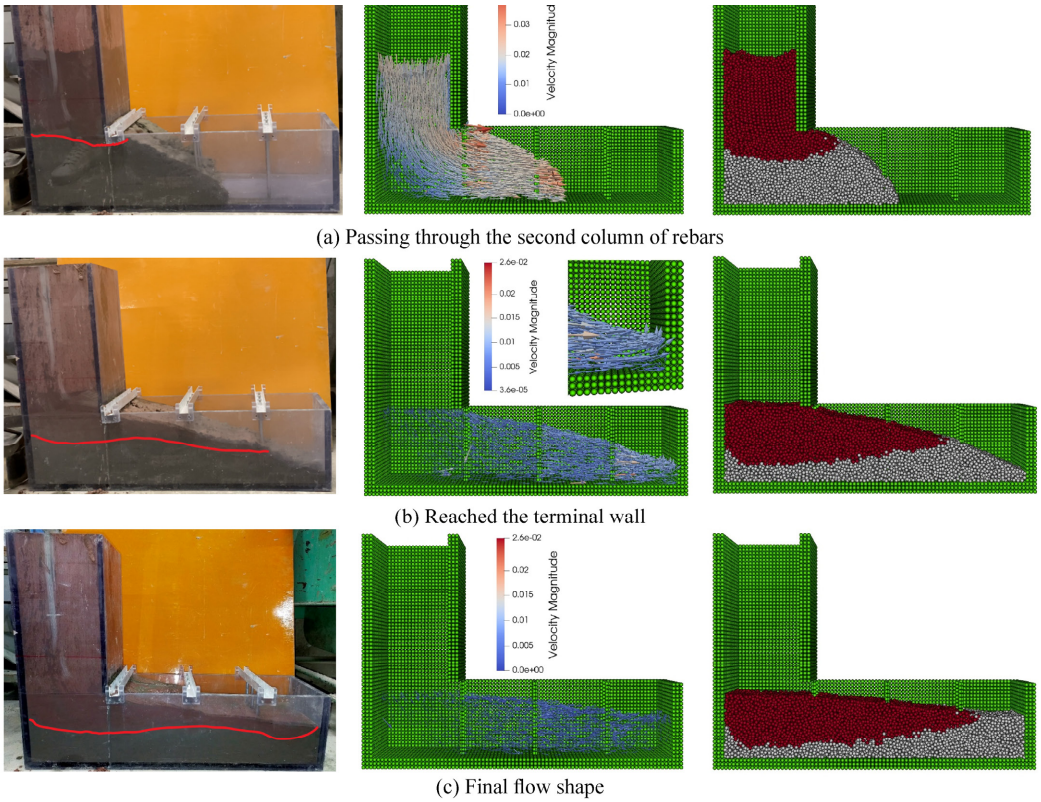

(a) Passing through the second column of rebars

(b) Reached the terminal wall

(c) Final flow shape

Fig. 12 Flow shape (left), velocity vector distribution (middle), and position change (right) of No. 1 at different times.

volume fraction of concretes, i.e., initial CA volume fraction, was 34% before the L-flow. For the crushed stone concrete, the measured CA volume fraction of the lower layer concrete was not smaller than 34% in zones A, B, and C, while the upper layer concrete had a smaller CA volume fraction of less than 34%, as shown in **Fig. 13(a)**. This is due to the higher density of crushed stone compared to the matrix mortar, causing the coarse aggregate to move downward under its gravity. As explained earlier, because the lower layer concrete located in zone C was pushed to move forward and upward in zone D, the difference in the CA volume fraction between the upper and lower layer concrete in zone D was smaller. Conversely, as shown in **Fig. 14(a)** the density of the LCA was lower than that of the matrix mortar, resulting in a greater CA volume fraction in the upper layer compared to the lower layer.

The CA volume fractions of the upper and lower layers of concrete in each zone, obtained from the numerical simulations were very close to the experimental results in the case of the LCA concrete, whether by the SI/DPMP method or by the DPMP method, as shown in **Figs. 14(b)** and **14(c)**. However, in the case of the crushed stone concrete, both the simulation methods gave larger CA volume fractions for the lower layer concrete than the experimental results, especially in zone D, as shown in **Figs. 13(b)** and **13(c)**. Maybe this is because of the densities of mortar and CA were strictly distinguished in the simulations, and the density of CA was greater than that of mortar, so the calculated volume fraction of CA in the lower layer of concrete was large. However, in the L-flow experiment, some small CA particles may be wrapped by matrix mortar and become part of the mortar, which increases the density of the mortar. On the contrary, some mortar adhered to the surfaces of CA particles (Kennedy 1940), which reduced the density of CA particle assembly. Thus, the CA segregation in the vertical direction was reduced.

4.3.2 CA distribution in the horizontal direction after the L-flow

Figure 15 shows the experimental and simulation results of CA volume fraction in four zones for the two concretes after the L-flow. In order to compare in detail, the differences in the accuracy of the two numerical methods for analyzing segregation in the flow direction of concrete, the deviation R_e of CA volume fractions obtained by the two numerical simulation methods, compared to the experimental results, were calculated respectively by Eq. (20), as shown in **Table 9**.

$$R_e = \sqrt{\frac{\sum_{\mathrm{A}}^{\mathrm{D}}\left(V_s^i - V_t^i\right)^2}{4}} \tag{20}$$

where V_s^i is the CA volume fraction in zone i based on the simulation, and V_t^i is the CA volume fraction in

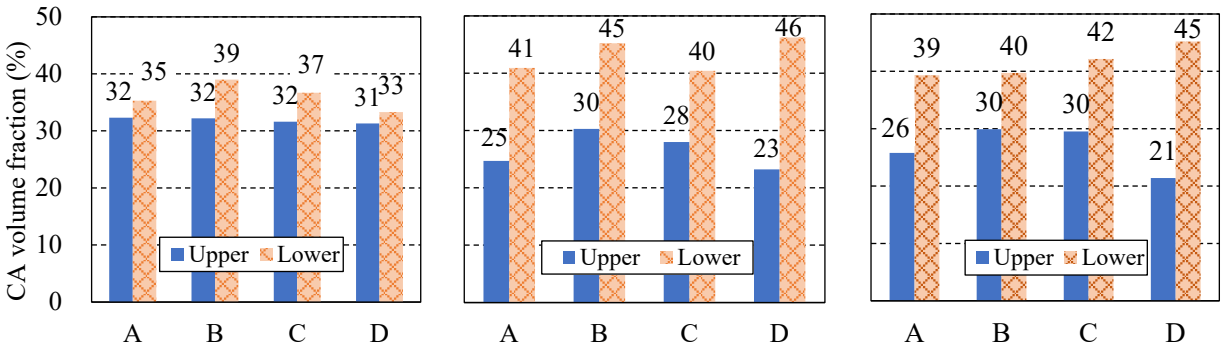

(a) Experiment (b) SI/DPMP method (c) DPMP method

Fig. 13 Segregation of the crushed stone concrete in the vertical direction.

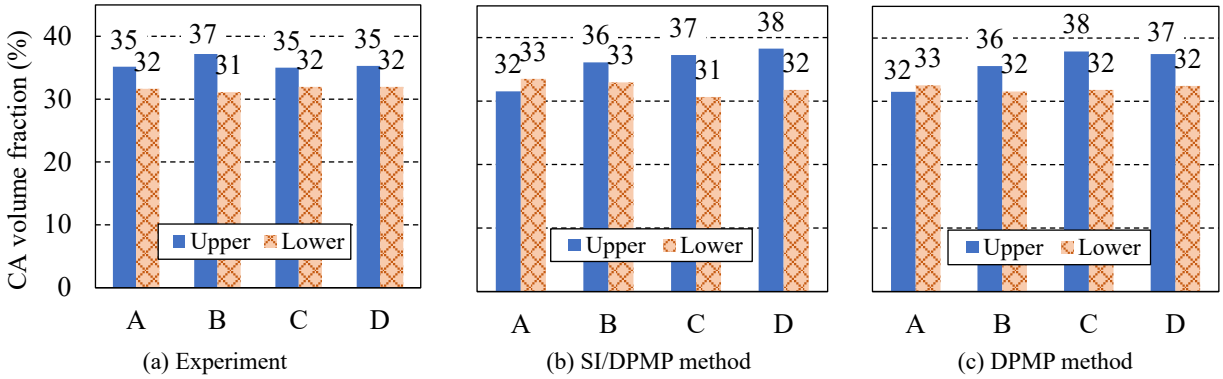

(a) Experiment (b) SI/DPMP method (c) DPMP method

Fig. 14 Segregation of the LCA concrete in the vertical direction.

Table 9 The deviation of simulation result compared to the experimental result.

	SI/DPMP	DPMP
No. 1	1.5	1.9
No. 2	1.1	1.3

zone i measured by the experiment.

The R_e of series No. 1 using the crushed stone as coarse aggregate demonstrates that the SI/DPMP method more accurately simulated the crushed stone segregation, compared to the DPMP method. The R_e of series No. 2 using the LCA also indicates that the SI/DPMP method was more accurate than the DPMP method, but the difference in simulation results between the two methods was small. The LCA particles were similar in shape, being mostly circular and elliptical, and the DPMP method forms the CA using the spherical envelope method, so the difference between the two numerical methods is minimal.

The crushed stone was collected from the concrete in each zone after the L-flow experiment, and after the simulation using the SI/DPMP method, respectively, and further divided into large particles with a diameter > 15 mm (initial volume fraction: 25.6%) and small particles with a diameter ≤ 15 mm (initial volume fraction: 74.4%). The massive ratio of two gradings of CA in each zone is shown in **Fig. 16**.

The ratio of large CA particles gradually decreased from zone B to zone D, while the number of small particles gradually increased. This trend is mainly due to the masses of the large particles, which caused a sharp decrease in momentum when encountering the rebars. Additionally, the large static inertia of the large particles made it difficult to move far. Conversely, smaller particles easily passed through the intervals of the rebars and were more easily entrained forward by their surrounding mortar.

Since the concrete sample filled in the vertical room stood for about 1 minute before the L-flow experiment started, static segregation of concrete might occur, thus the ratio of large particles in the upper part of the concrete decreased. During the L-flow, the upper part of the concrete settled down and remained in zone A, resulting in a smaller ratio of large particles in zone A, compared to

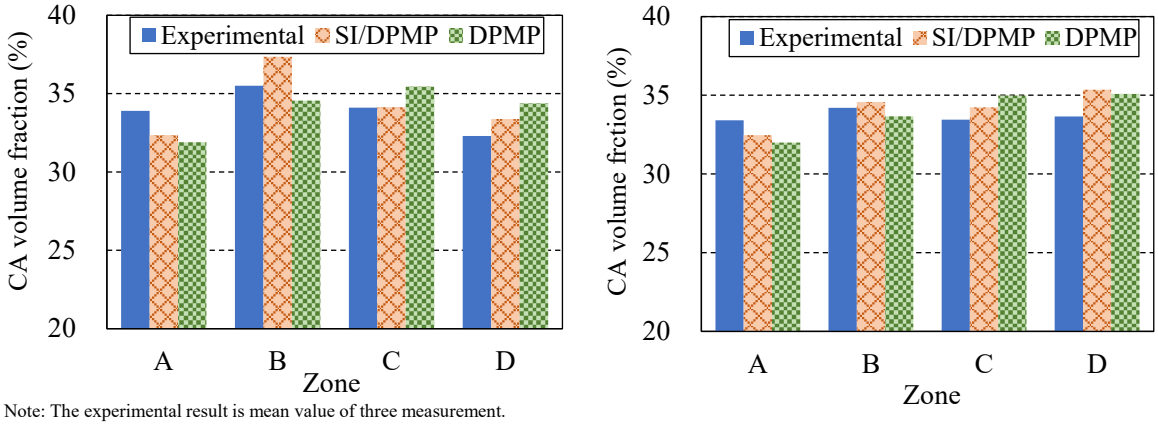

Note: The experimental result is mean value of three measurement.

(a) Crushed stone concrete (No. 1) (b) Lightweight aggregate concrete (No. 2)

Fig. 15 CA segregation in the horizontal direction.

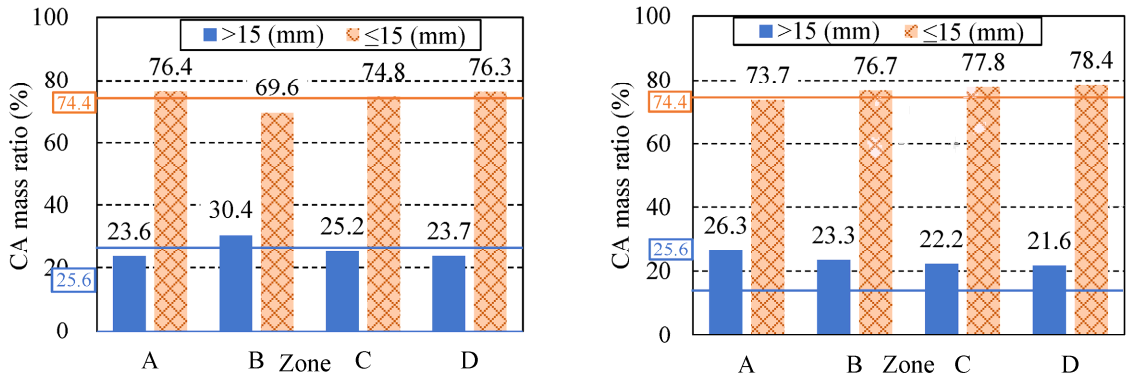

(a) Experimental results (b) Simulation results by the SI/DPMP method

Fig. 16 Distribution of CA particles with different gradings in horizontal direction.

zone B. However, in the present numerical analysis, the static segregation before the box gate was lifted was not considered, so the large particles had a greater ratio in zone A than in zone B. Overall, the results of the numerical analysis of segregation in the horizontal direction were in good agreement with the experimental results.

5. Summary and conclusions

In order to establish a flow simulation-based workability design technology for the placement of reinforced self-consolidating concrete, a new numerical approach, called the SI/DPMP method was developed in this study. This method was built upon the moving particle complete-implicit (I-MPS), in which the fresh concrete is treated as a two-phase granular fluid comprising matrix mortar and coarse aggregate (CA). This new numerical approach forms CA particles with small spherical elementary particles according to CA's fineness modulus, PSD, and shape index determined through permeability testing. Additionally, the constraint effect of rebars was considered by introducing stress perpendicular to shear stress. Through experimental and numerical investigations of the flow and segregation behaviors of two types of high-fluidity concrete in an L-shaped box with rebars, the following conclusions can be obtained:

(1) The proposed SI/DPMP method produced the numerical results closer to the experimental results on the flow and segregation behaviors during casting reinforced SCC, compared to the traditional MPS and the original DPMP method, regardless of whether ordinary aggregate or lightweight aggregate was used as CA.
(2) Most of the concrete, located initially in the lower position, will flow to the front. If it reaches the end and meets an obstacle, it will turn back upward.
(3) When the coarse aggregate has a smaller shape index (worse shape), the SI/DPMP method that considers the CA shape can provide a more precise simulation than the original DPMP method. On the contrary, when the CA particles are near spheres, the improvement of simulation accuracy using the SI/DPMP method is limited.
(4) During concrete flow, normal crushed stone CA particles tend to settle down, the lower part of the concrete has more CA particles, while the lightweight coarse aggregate floats upward, there are more CA particles in the upper part of the concrete. In the horizontal direction, the distribution of lightweight CA particles is more uniform than that of crushed stone aggregate.
(5) The traditional MPS using the single-phase & mono-particle (SPMP) model is suitable for simulating the concrete placement without the need to predict segregation behavior. The MPS using the original DPMP model is better suited for predicting the flow and segregation behaviors of fresh concrete with near-spherical coarse aggregates, such as gravel and artificial aggregate. The MPS using the SI/DPMP model is applied to the simulations of the flow and segregation of fresh concrete using crushed stone as coarse aggregate.

The current numerical method is not yet able to deal with deformed rebar, thus the rounded rebars were used in this study. In the future, we will further discuss the numerical expression of the influence of deformed rebar. After improving this numerical method, we will combine it with Building Information Modeling (BIM) for the automatic input of concrete flow boundary and reinforcement configuration, and the visualization of concrete filling and segregation prior to the construction, which will ultimately realize the workability design of concrete based on flow simulation.

References

ACI, (2007). "*Self-consolidating concrete* (ACI 237R-07)." West Conshohocken, Pennsylvania: American Concrete Institute.

Cao, G. and Li, Z., (2017). "Numerical flow simulation of fresh concrete with viscous granular material model and smoothed particle hydrodynamics." *Cement and Concrete Research*, 100, 263-274.

Cao, G., Li, Z. and Guo, K., (2017). "Analytical study on the change of fluidity of fresh concrete containing mineral admixture with rest time." *Journal of Advanced Concrete Technology*, 15(11), 713-723.

Cao, G., Li, Z. and Xu, Z., (2019). "A SPH simulation method for opening flow of fresh concrete considering boundary restraint." *Construction and Building Materials*, 198, 379-389.

Cao, G., Liu, Y., Long, S., Deng, D., Jiang, S., Su, H. and Tan, T., (2023). "Influence of aggregate shape on the flow properties of fresh concrete." *Powder Technology*, 415, 118186.

Cepuritis, R., Jacobsen, S., Pedersen, B. and Mørtsell, E., (2016). "Crushed sand in concrete - Effect of particle shape in different fractions and filler properties on rheology." *Cement and Concrete Composites*, 71, 26-41.

Chateau, X., Ovarlez, G. and Trung, K. L., (2008). "Homogenization approach to the behavior of suspensions of noncolloidal particles in yield stress fluids." *Journal of Rheology*, 52(2), 489-506.

Chu, H., Machida, A. and Kobayashi, H., (1997). "Verification of application of DEM to fresh concrete by sphere dragging viscometer." *Transactions of the Japan Concrete Institute*, 19, 463-468. (in Japanese)

Cui, W., Yan, W.-S., Song, H.-F. and Wu, X.-L., (2020). "DEM simulation of SCC flow in L-box set-up: Influence of coarse aggregate shape on SCC flowability." *Cement and Concrete Composites*, 109, 103558.

Duan, G., Chen, B., Koshizuka, S. and Xiang, H., (2017). "Stable multiphase moving particle semi-implicit method for incompressible interfacial flow." *Computer Methods in Applied Mechanics and Engineering*, 318,

636-666.

Ferraris, C. F. and De Larrard, F., (1998). "*Testing and modeling of fresh concrete rheology*." Gaithersburg, Maryland: National Institute of Standards and Technology (NIST).

Ferraris, C. F., De Larrard, F. and Martys, N., (2001). "*Fresh concrete rheology: Recent developments*." Gaithersburg, Maryland: National Institute of Standards and Technology (NIST).

Galbusera, F. and Niemeyer, F., (2018). "Mathematical and finite element modeling." In: *Biomechanics of the Spine*. Cambridge, Massachusetts: Academic Press, Section 3, 239-255.

Hu, J. and Wang, K., (2011). "Effect of coarse aggregate characteristics on concrete rheology." *Construction and Building Materials*, 25(3), 1196-1204.

Kennedy, C. T., (1940). "The design of concrete mixes." *ACI Journal Proceedings*, 36(2), 373-400.

Khayat, K. and Mitchell, D., (2009). "*Self-consolidating concrete for precast, prestressed concrete bridge elements*." Washington DC: US Transportation Research Board.

Koshizuka, S. and Oka, Y., (1996). "Moving-particle semi-implicit method for fragmentation of incompressible fluid." *Nuclear Science and Engineering*, 123(3), 421-434.

Krieger, I. M. and Dougherty, T. J., (1959). "A mechanism for non-Newtonian flow in suspensions of rigid spheres." *Journal of Rheology*, 3(1), 137-152.

Li, J. and Li, Z., (2011). "Effect of boundary restraint on flow of fresh concrete though opening." *AIJ Journal of Structural and Construction Engineering*, 76(665), 1189-1197.

Li, Y., Mu, J., Wang, Z., Liu, Y. and Du, H., (2021). "Numerical simulation on slump test of fresh concrete based on lattice Boltzmann method." *Cement and Concrete Composites*, 122, 104136.

Li, Z., (2007). "State of workability design technology for fresh concrete in Japan." *Cement and Concrete Research*, 37(9), 1308-1320.

Li, Z., (2014). "Evaluating method for particle geometry of aggregate." *AIJ Journal of Technology and Design*, 20(46), 839-844. (in Japanese)

Li, Z., (2015). "Rheological model and rheometer of fresh concrete." *AIJ Journal of Structural and Construction Engineering*, 80(710), 527-537. (in Japanese)

Li, Z., (2022). "Rheological model of fresh concrete considering granular characteristics." *Composites Part B: Engineering*, 244, 110148.

Li, Z. and Iidaka, M., (2020). "Development of rheological measurement method for fresh concrete considering its granular characteristic." In: *Proc. 6th International Conference on Construction Materials: Performance, Innovations and Structural Implications*, Fukuoka, Japan 27-29 August 2020. Tokyo: Japan Concrete Institute, 1456-1467.

Lucy, L. B., (1977). "A numerical approach to the testing of the fission hypothesis." *Astronomical Journal*, 82, 1013-1024.

Monaghan, J. J., (1994). "Simulating free surface flows with SPH." *Journal of Computational Physics*, 110(2), 399-406.

Murata, J. and Suzuki, K., (1987). "Study on grout flow in pipe with sliding at wall." *Doboku Gakkai Ronbunshu*, 384/V-7, 129-136. (in Japanese)

Ozawa, K., (1989). "High-performance concrete based on the durability design of concrete structures." In: *Proc. 2nd East Asia-Pacific Conference on Structural Engineering and Construction*, Chiang Mai, Thailand 11-13 January 1989. Bangkok: Asian Institute of Technology.

Roscoe, R., (1952). "The viscosity of suspensions of rigid spheres." *British Journal of Applied Physics*, 3(8), 267-269.

Roussel, N. and Gram, A., (2014). "*Simulation of fresh concrete flow* (RILEM TC 222-F State of the art report)." Dordrecht: Springer.

Roussel, N., Nguyen, T. L. H., Yazoghli, O. and Coussot, P., (2009). "Passing ability of fresh concrete: A probabilistic approach." *Cement and Concrete Research*, 39(3), 227-232.

Sakihara, K., Iraha, S., Iribe, T. and Tomiyama J., (2004). "Flow analysis of fresh concrete using SPH method." *Proceedings of the Japan Concrete Institute*, 26(1), 1149-1154. (in Japanese)

Shakibaeinia, A. and Jin, Y.-C., (2012). "MPS mesh-free particle method for multiphase flows." *Computer Methods in Applied Mechanics and Engineering*, 229-232, 13-26.

Struble, L. J. and Sun, G.-K., (1992). "Cement viscosity as a function of concentration." *MRS Online Proceedings Library*, 289, 173-178.

Sun, X., Sakai, M., Shibata, K., Tochigi, Y. and Fujiwara, H., (2012). "Numerical modeling on the discharged fluid flow from a glass melter by a Lagrangian approach." *Nuclear Engineering and Design*, 248, 14-21.

Tanigawa, Y. and Mori, H., (1988). "Toward the development of workability design of fresh concrete." *Cement Concrete*, 501, 11-20. (in Japanese)

Teranishi, K. and Tanigawa, Y., (2007). "Effect of aggregate grading on fluidity of concrete and mortar." *AIJ Journal of Structural and Construction Engineering*, 72(614), 9-16. (in Japanese)

Uehara, Y., Yamada, Y., Sakihara, K. and Urano, S., (2015). "A basic study on the segregation simulation by using MPS method." *Cement Science and Concrete Technology*, 69(1), 711-717. (in Japanese)

Wang, Z., Hao, J., Li, Y. and Tian, X., (2022). "Simulation of concrete pumped in horizontal coil and super high-rise building based on CFD." *Journal of Advanced Concrete Technology*, 20(4), 328-341.

Xu, Z. and Li, Z., (2021). "Numerical method for predicting flow and segregation behaviors of fresh concrete." *Cement and Concrete Composites*, 123,

104150.

Xu, Z., Li, Z. and Jiang, F., (2021). "The applicability of SPH and MPS methods to numerical flow simulation of fresh cementitious materials." *Construction and Building Materials*, 274, 121736.

Xu, Z., Li, Z., Liu, J., Chen, W., Liu, J. and Han, F., (2024). "Test method of segregation resistance of high fluidity concrete based on numerical simulation of dynamic segregation of coarse aggregate." *Journal of Advanced Concrete Technology*, 22(6), 372-382.

Yamada, Y., Uehara, Y., Sakihara, K. and Urano, S., (2020). "Slump flow simulation of high fluidity concrete by MPS method." *AIJ Journal of Structural and Construction Engineering*, 85(771), 663-672. (in Japanese)

Zhao, Y., Duan, Y., Zhu, L., Wang, Y. and Jin, Z., (2021). "Characterization of coarse aggregate morphology and its effect on rheological and mechanical properties of fresh concrete." *Construction and Building Materials*, 286, 122940.

Zhu, H., Martys, N. S., Ferraris, C. and De Kee, D., (2010). "A numerical study of the flow of Bingham-like fluids in two-dimensional vane and cylinder rheometers using a smoothed particle hydrodynamics (SPH) based method." *Journal of Non-Newtonian Fluid Mechanics*, 165(7), 362-375.